Nagurka, M.L. and Wang, S.K.., "Modeling a Superconducting Maglev Vehicle/Guideway System," Proceedings of the Tenth VPI&SU/AIAA Symposium on Dynamics and Control of Large Structures, Blacksburg, VA, May 8-10, 1995, pp.355-366.

MODELING A SUPERCONDUCTING MAGLEV VEHICLE/GUIDEWAY SYSTEM

M. Nagurka and S.-K. Wang
Carnegie Mellon Research Institute
Pittsburgh, PA 15230

Abstract

This study investigates the dynamic interactions between magnetically levitated (maglev) vehicles employing electromagnetic suspension (EMS) systems and elevated flexible guideways. In EMS designs, vehicle levitation and guidance is achieved by attraction between vehicle-borne magnets and iron rails mounted to the guideway. EMS maglev systems rely on feedback control to actively position the vehicle on the guideway to achieve a nominal air gap and ensure overall safe performance. Furthermore, the control system plays a critical role in providing acceptable passenger ride comfort.

The objective of this work is to develop a computer simulation model for predicting the dynamic performance of a superconducting (SC) EMS maglev vehicle operating over a flexible, multiple span, elevated guideway. A sequence of dynamic component models is developed. For example, a magnet model is derived which characterizes the behavior of the on-board SC magnets. A five degree of freedom (DOF) nonlinear vehicle model, representing lateral, vertical, roll, pitch, and yaw motions, is also developed. The vehicle's magnet modules are controlled using linear quadratic (LQ) optimal control augmented with integral action to avoid steady-state gap errors which might otherwise arise from guideway offsets or constant cross-wind gusts.

A simply supported, multi-spanned, tangent guideway model is proposed to evaluate vehicle dynamic response for a range of guideway geometry inputs and wind force inputs. In addition to the cross-wind gust, the disturbances imposed on the maglev system include guideway deflection due to inherent span compliance and guideway irregularities such as random roughness and offsets (steps, ramps, and camber irregularities). The design criteria is to minimize the gap errors and passenger accelerations without exceeding limits on the controlled voltage of the magnet modules.

The computer model is used in simulation studies to provide insights into the nature of the dynamic interaction expected in high speed EMS maglev operation. To achieve acceptable performance in terms of safety, ride quality, and power demand, maglev designs require detailed dynamic analyses that account for the governing behavior of their magnet modules, vehicle and guideway DOFs, and controller structure as well as the interaction coupling the vehicle, guideway, and control subsystems.

1. Introduction

Maglev vehicles are one class of high-speed guided ground transportation vehicles being considered for deployment in the U.S. Unlike conventional trains that use wheels and rails, maglev vehicles are generally suspended above an elevated guideway by magnet forces. In addition to levitation, magnet forces are employed to guide the vehicle (*i.e.*, center it within or over the guideway), propel the vehicle along the guideway, and assist in braking action. The non-contact operation of maglev vehicles is distinct from conventional rail vehicles relying on mechanical stresses and friction forces between steel rails and wheels.

In the United States, the National Maglev Initiative (NMI) has been established to assess the role of maglev high speed transportation in the Nation's future. Four System Concept Definitions have been developed under the NMI. Among them the designs of Bechtel, Foster-Miller, and Magneplane are electro-dynamic suspension systems that rely upon "repulsive" magnet forces. Grumman's system concept is an electromagnetic suspension (EMS) system employing "attractive" forces and superconducting (SC) magnets.

Many types of maglev system models have been proposed and analyzed. For example, Wormley, *et al.*

(1992) used simplified one-dimensional vehicle models for providing initial guidelines and overall directions for maglev design and development. Dynamic interactions between a maglev vehicle and a flexible guideway were studied in (Cai, *et al.*, 1994) using a two DOF vehicle model. More sophisticated vehicle models were developed for maglev systems in (Daniels, *et al.*, 1992) to evaluate vehicle/guideway interactions for various guideway structures. The vehicle/guideway interactions of a maglev system with a multi-car, multi-load vehicle were investigated in (Cai, *et al.*, 1993).

An objective of this study is to develop a detailed mathematical model for evaluating the dynamics of a SC EMS-type maglev vehicle with a combined lift and guidance system. The aim of the mathematical model is to simulate the maglev vehicle over a multi-span flexible guideway at full speed under the influence of guideway irregularities and aerodynamic loading. The overall system can be decomposed into four main components: vehicle model, magnet model, guideway model, and controller. The purpose of this paper is to describe detailed mathematical models of these subsystems.

2. System Models

2.1 Vehicle Model

In order to facilitate the development of the vehicle model, two coordinate systems, an inertial coordinate frame and a carbody coordinate frame, are first established. The carbody motion is then described by the translational and rotational transformations between these two coordinate systems. The carbody coordinate frame is fixed in the vehicle carbody with principal axes X_C, Y_C, and Z_C and origin located at the vehicle center of gravity identified as CG. The inertial coordinate frame, $X_I Y_I Z_I$, moves along the guideway longitudinal direction (*i.e.*, X_I direction) at a constant vehicle speed, V_v.

The vehicle motion is characterized by the lateral and vertical displacements of the carbody CG and the roll, pitch, and yaw angles which describe the orientation of the carbody coordinate frame with respect to the inertial frame. The lateral and vertical displacements of the carbody CG are denoted by y_c and z_c, respectively. It is assumed that the carbody axes are initially aligned with the inertial reference axes. Then, the orientation of the carbody frame can be reached by successive rotations as follows: (*i*) a rotation ψ_c (yaw) about the Z_C axis, (*ii*) a rotation θ_c (pitch) about the resulting Y_C axis, and (*iii*) a rotation ϕ_c (roll) about the resulting X_C axis.

A maglev vehicle model is developed based on the Grumman system concept (Proise, *et al.*, 1993). Figure 1 shows the vehicle in its nominal position. There are N_m magnet modules on each side, inclined at angle β from vertical. (N_m is an even number.) The magnets are arranged in such a way that the magnet forces pass through the longitudinal axis of the vehicle when the vehicle is in its nominal position. Each module contains several magnets controlled by the same power supply. The magnet force at each magnet module is assumed to be distributed uniformly along the module length, l_m. The vehicle carbody is assumed to be rigid. The vehicle length and height are denoted by L_v and h_v, respectively. Also shown in the figure are the nominal air gap, h_0, and the height and width between the module and the carbody CG, denoted by h_c and w_c, respectively.

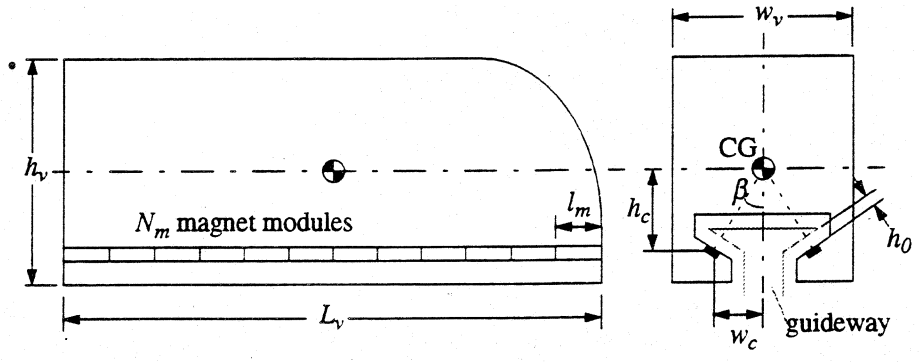

Figure 1. Grumman-Type Vehicle Configuration

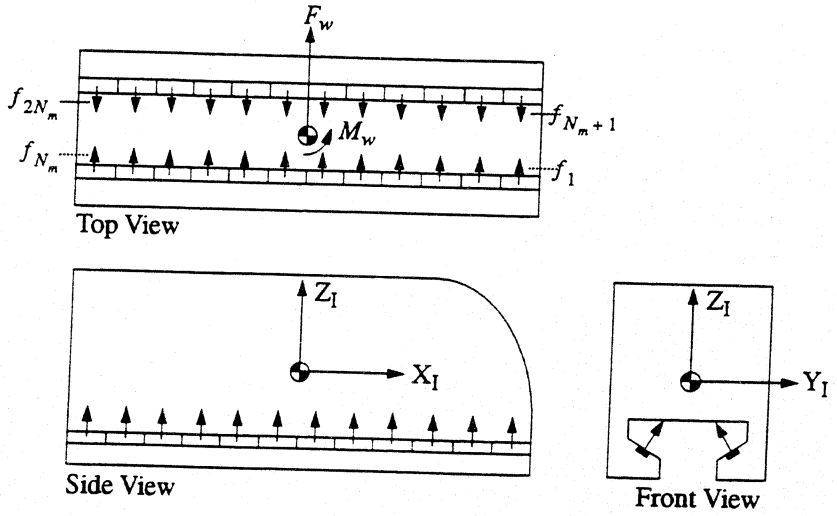

Figure 2. Free-Body Diagram of Vehicle Carbody

The free-body diagram of the vehicle carbody is shown in Figure 2. The vehicle is supported by magnet forces from the two rows of magnet modules. In addition to the magnet forces, the vehicle model described here may be disturbed by a cross-wind gust represented by an aerodynamic force, F_w, in the lateral direction and an aerodynamic moment, M_w, in the yaw direction. The vehicle model equations of motion can be written as

$$F_y + F_w = M_v \ddot{y}_c \tag{1}$$

$$F_z - M_v g = M_v \ddot{z}_c \tag{2}$$

$$M_x = I_x \dot{\omega}_x - (I_y - I_z)\,\omega_y \omega_z \tag{3}$$

$$M_y = I_y \dot{\omega}_y - (I_z - I_x)\,\omega_z \omega_x \tag{4}$$

$$M_z + M_w = I_z \dot{\omega}_z - (I_x - I_y)\,\omega_x \omega_y \tag{5}$$

$$\dot{\phi}_c = \omega_x + (\omega_y \phi_c + \omega_z)\,\theta_c \tag{6}$$

$$\dot{\theta}_c = \omega_y - \omega_z \phi_c \tag{7}$$

$$\dot{\psi}_c = \omega_y \phi_c + \omega_z \tag{8}$$

where M_v is the vehicle mass, g is the acceleration due to gravity, I_x, I_y, and I_z are the roll, pitch, and yaw moments of inertia of the vehicle, respectively, and ω_x, ω_y, and ω_z are the roll, pitch, and yaw angular velocities, respectively, in the carbody coordinate frame. Equations (1) and (2) are the translational equations of motion given by Newton's second law, where F_y and F_z are the total magnet force components in the lateral and vertical directions, respectively, applied to the carbody CG. Equations (3)-(5) are the rotational equations of motion from Euler's equations, where M_x, M_y, and M_z are the resultant roll, pitch, and yaw moments due to the magnet forces. Equations (6)-(8) are the angle-angular velocities relations which couple the vehicle angular velocities to the roll, pitch, and yaw angles, where small angles are assumed. The magnet forces, F_y and F_z, and the corresponding moments, M_x, M_y, and M_z, have been derived in (Wang, 1995).

2.2 SC Magnet Model

The proposed Grumman vehicle design contains forty-eight EMS-type SC magnets, twenty-four magnets on each side (Proise, *et al.*, 1993). In this study, the vehicle magnets are grouped into $2N_m$ magnet modules. All magnets in a module are controlled by a single power supply. The number of magnet modules is a design variable and can be specified based on the required dynamic performance.

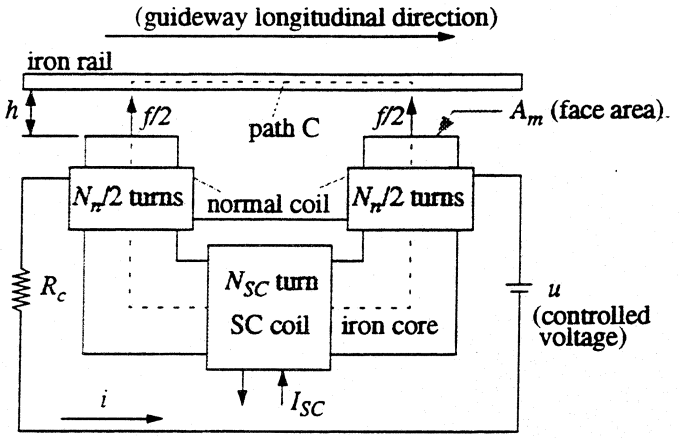

Figure 3. SC Magnet Configuration

The SC magnet system, shown schematically in Figure 3, consists of a guideway iron rail, an iron-core magnet, a SC coil wrapped on the back leg of the iron core, and a set of normal coils, which are serially connected, attached to both pole ends of the iron core. N_{SC} and N_n are the numbers of turns in the SC coil and the normal coils, respectively. The current in the SC coil, I_{SC}, is provided by a constant current source, and the resulting magnet force provides the lifting capability to balance the total weight in static equilibrium. The trim current, i, in the normal coils is driven by a controlled voltage, u, to maintain the air gap, h, at its nominal value. The total magnet force provided by the magnet is f. The total resistance of the normal coils is denoted by R_c and the face area of each magnetic pole is denoted by A_m.

By applying Ampere's law along path C in Figure 3 and using the law of conservation of energy for the magnetic energy stored in the air gap, the attractive magnet force at magnet module j can be represented as

$$f_j = \frac{\mu_0 A_m n_m}{4h_j^2}(N_{SC}I_{SC} + N_n i_j)^2, \quad j = 1, \ldots, 2N_m \tag{9}$$

where μ_0 is the permeability of air, n_m is the number of magnets in each magnet module, and h_j and i_j are the air gap and trim current at module j, respectively. From Kirchhoff's voltage law, the trim current/voltage relation in magnet module j can be derived as

$$u_j = R_c i_j + \frac{\mu_0 A_m N_n^2}{2h_j}\frac{di_j}{dt} - \frac{\mu_0 A_m N_n (N_{SC}I_{SC} + N_n i_j)}{2h_j^2}\frac{dh_j}{dt}, \quad j = 1, \ldots, 2N_m \tag{10}$$

In summary, the dynamics of the SC magnet model are described by the voltage equation (10) for each module and can be represented by $2N_m$ first-order ODEs. The resulting trim current and the constant SC current in each magnet module produce a magnetic flux which set up the attractive magnet force between the iron core and the iron rail. The magnet force at each module, described by Equation (9), is a nonlinear function of the trim current, SC current, and air gap between the magnet and the rail.

2.3 Guideway Model

The guideway deviations at the magnet modules can be attributed to vehicle dynamic loading on the flexible guideway spans and to guideway geometry irregularities. The guideway model, developed here, relates the magnet force and the corresponding guideway deflection for each magnet module. A multi-span, elevated guideway is considered. Figure 4 shows the guideway configuration for a single span. The guideway span consists of the track slab which contains the iron rails and a box beam which is simply supported. The box beam selected in this study is the narrow, hollow-box beam (Phelan, 1993). A benefit of the narrow beam design for vehicles with inclined magnets is that it reduces the distance between the right- and left-side magnets and thus a smaller cant angle is allowed for providing levitation with a smaller magnet force.

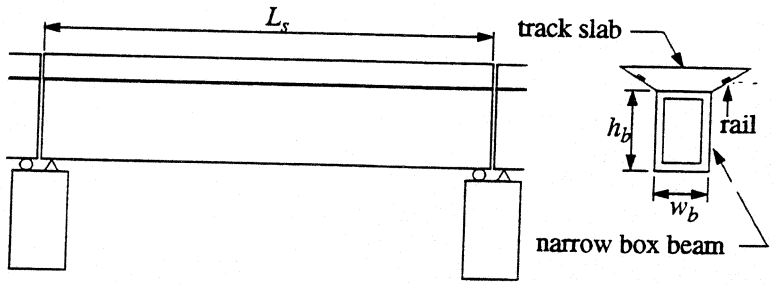

Figure 4. Guideway Span Configuration

A Bernoulli-Euler beam with simply supported ends is assumed to model each guideway span. The equation of motion for a span can be expressed as

$$EI\frac{\partial^4}{\partial x_s^4}\tilde{w}_s(x_s,t) + c\frac{\partial}{\partial t}\tilde{w}_s(x_s,t) + \gamma\frac{\partial^2}{\partial t^2}\tilde{w}_s(x_s,t) = \tilde{f}(x_s,t) \tag{11}$$

where x_s is the axial coordinate of the beam, t is time, EI is the bending rigidity, c is the viscous damping coefficient, γ is the mass per unit length of the beam, $\tilde{w}_s(x_s,t)$ is the vertical deflection of the beam, and $\tilde{f}(x_s,t)$ is the loading force per unit length due to the moving vehicle acting on the beam. (The use of the superscript ~ denotes functional dependence on both space and time.)

To determine the solution of Equation (11), a modal analysis method is utilized in which the deflection of the beam is expressed as

$$\tilde{w}_s(x_s,t) = \sum_{j=1}^{n_s} a_j(t)\sin(j\pi x_s/L_s) \tag{12}$$

where $a_j(t)$ is the time-varying modal amplitude, L_s is the span length, $\sin(j\pi x_s/L_s)$ is the mode shape of the simply supported beam, and n_s is the number of mode shapes included in the solution. Substituting Equation (12) into Equation (11) and then multiplying by $\sin(k\pi x_s/L_s)$ and integrating from $x_s=0$ to $x_s=L_s$ gives the resulting differential equation for the modal amplitude $a_j(t)$ as

$$\ddot{a}_j(t) + \frac{c}{\gamma}\dot{a}_j(t) + \frac{EI}{\gamma}\left(\frac{j\pi}{L_s}\right)^4 a_j(t) = \frac{2}{\gamma L_s}\int_0^{L_s}\tilde{f}(x_s,t)\sin\left(\frac{j\pi x_s}{L_s}\right)dx_s \tag{13}$$

with initial condition, $a_j(0)=a_{j0}$, for $j=1,...,n_s$. From Equation (13), the circular frequency and the modal damping ratio can be identified as

$$\omega_j = \frac{j^2\pi^2}{L_s^2}\sqrt{\frac{EI}{\gamma}}, \qquad \zeta_j = \frac{c}{2\gamma\omega_j} \tag{14)-(15}$$

for $j=1,...,n_s$. The beam deflection can be determined by Equation (12) after solving Equation (13).

The vehicle is assumed to negotiate a multi-span guideway as depicted in Figure 5. The vehicle/guideway interaction is considered in the time interval $[t_0, t_f]$. At $t=t_0$, the vehicle is completely located on Span I and just about to enter Span II. As time increases, the vehicle excites both Span I and Span II simultaneously. In this study, it is assumed that the vehicle length, L_v, is less than the guideway span length, L_s. As a result, the vehicle is completely located on Span II at $t=t_f$. For multi-span configurations, additional spans can be "daisy-chained" (*i.e.*, at $t=t_f$, the clock is reset to $t=t_0$ and the same algorithm for the following span is applied).

The dynamic interaction between a moving vehicle and a flexible guideway has been studied intensively (*e.g.*, Kortum and Wormley, 1981; Smith and Wormley, 1974). The process of deriving the vehicle/guideway

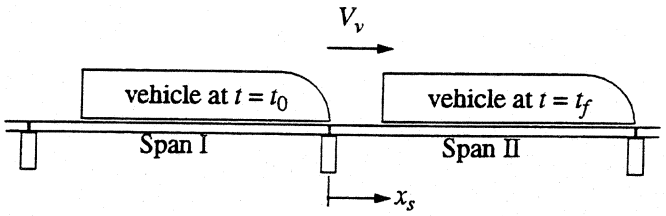

Figure 5. Vehicle Traversing Guideway Spans

interaction involves three steps. The first step is to convert the magnet forces on the modules into the distributed loading forces on Span I and Span II. It should be noted that the excitation on the spans is modeled as a distributed, time-varying moving force for the vehicle/guideway system in this study. The second step is to solve for the distributed span deflections. The final step is to obtain the guideway deflection observed at each module. Since the magnet forces applied to the guideway rails are distributed, the effective guideway displacement at each module is given by the average guideway displacement over the module length (Gran and Proise, 1993). The magnet module may be located entirely on Span I, on both Span I and Span II, or entirely on Span II. The corresponding deflections can be derived (Wang, 1995), respectively, as

$$w_{s,j}(t) = w_{s,j+N_m}(t) = \frac{1}{l_m}\int_{x_{l,j}}^{x_{u,j}} \tilde{w}_I(-\sigma, t)\, d\sigma, \qquad x_{s,j} \le -\frac{l_m}{2} \tag{16}$$

$$w_{s,j}(t) = w_{s,j+N_m}(t) = \frac{1}{l_m}\left[\int_{x_{l,j}}^{0} \tilde{w}_I(-\sigma, t)\, d\sigma + \int_{0}^{x_{u,j}} \tilde{w}_{II}(\sigma, t)\, d\sigma\right], \quad -\frac{l_m}{2} < x_{s,j} < \frac{l_m}{2} \tag{17}$$

$$w_{s,j}(t) = w_{s,j+N_m}(t) = \frac{1}{l_m}\int_{x_{l,j}}^{x_{u,j}} \tilde{w}_{II}(\sigma, t)\, d\sigma, \qquad x_{s,j} \ge \frac{l_m}{2} \tag{18}$$

where $\tilde{w}_I(\sigma, t)$ and $\tilde{w}_{II}(\sigma, t)$ are the guideway deflections on Span I and Span II, respectively, and

$$x_{s,j} = x_{s,j+N_m} = V_v t - j l_m + l_m/2 \tag{19}$$

$$x_{u,j} = x_{s,j} + l_m/2, \qquad x_{l,j} = x_{s,j} - l_m/2 \tag{20)-(21}$$

In summary, the input to the guideway model is the magnet force at each magnet module and the output is the corresponding guideway deflection. The guideway dynamic analysis considers the first n_s modes of beam vibration and thus the governing equations consist of $2n_s$ second-order ODEs for two spans. The guideway model accounts for two sequential spans and then concatenates them for guideways involving multiple (*i.e.*, greater than two) spans.

3. Control Scheme

A key goal of the controller is to stabilize the EMS system. Further, the controller must successfully reject disturbances while regulating the air gap. In this work, an LQ optimal control strategy with integral action is applied to minimize the passenger accelerations without exceeding limits on air gap variations.

The proposed control method requires a linearized plant model to design the control law. The nonlinear plant model, including the vehicle and magnet modules, is first linearized about its nominal operating point (*i.e.*, the trim currents, vehicle displacements and velocities are set to zero and the air gap at each magnet module is set to the nominal air gap, h_0). To eliminate non-zero steady-state gap errors due to constant disturbances, the linear plant is augmented by adding integrators at its outputs. The resulting augmented plant can be represented

as (Wang, 1995)

$$\dot{\mathbf{x}} = \mathbf{A}\mathbf{x} + \mathbf{B}\mathbf{u} + \mathbf{E}\mathbf{v} \tag{22}$$

$$\mathbf{y} = \mathbf{C}\mathbf{x} + \mathbf{D}\mathbf{v} \tag{23}$$

where the augmented state vector, **x**, control vector, **u**, output vector **y**, and disturbance vector, **v**, can be identified as

$$\mathbf{x} = [y_c, z_c, \phi_c, \theta_c, \psi_c, \omega_x, \omega_y, \omega_z, i_1, \ldots, i_{2N_m}, y_{I1}, \ldots, y_{I(2N_m)}]^T \tag{24}$$

$$\mathbf{u} = [u_1, \ldots, u_{2N_m}]^T \tag{25}$$

$$\mathbf{y} = [h_1 - h_0, \ldots, h_{2N_m} - h_0]^T \tag{26}$$

$$\mathbf{v} = [y_{g1}, \ldots, y_{g(2N_m)}, z_{g1}, \ldots, z_{g(2N_m)}, \dot{y}_{g1}, \ldots, \dot{y}_{g(2N_m)}, \dot{z}_{g1}, \ldots, \dot{z}_{g(2N_m)}, F_w, M_w]^T \tag{27}$$

where y_{Ij} (j=1,...,$2N_m$) is the integral of the air gap error at module j. The LQ optimal control law results from the minimization of the performance index,

$$J = \int_0^\infty \left(\mathbf{x}^T\mathbf{Q}\mathbf{x} + \mathbf{u}^T\mathbf{R}\mathbf{u} \right) dt \tag{28}$$

subject to $\dot{\mathbf{x}} = \mathbf{A}\mathbf{x} + \mathbf{B}\mathbf{u}$. When applied to the augmented plant model the optimal control law can be shown to be

$$\mathbf{u} = -\mathbf{R}^{-1}\mathbf{B}^T\mathbf{P}\mathbf{x}(t) \tag{29}$$

where **P** is a unique, symmetric, semi-positive definite matrix solved from the algebraic Riccati equation

$$\mathbf{P}\mathbf{A} + \mathbf{A}^T\mathbf{P} - \mathbf{P}\mathbf{B}\mathbf{R}^{-1}\mathbf{B}^T\mathbf{P} + \mathbf{Q} = \mathbf{O} \tag{30}$$

provided system (**A**, **B**) is stabilizable and system (**A**, **H**), where $\mathbf{H}^T\mathbf{H}$=**Q**, is detectable. In Equations (29) and (30), **Q** and **R** are two weighting matrices which can be adjusted to achieve desired closed-loop behavior.

4. Simulation Study

The complete maglev system, consisting of the vehicle model, guideway model, SC magnet system, and controller, is represented in the block diagram of Figure 6. The inputs to the overall system are the aerodynamic force and moment, F_w and M_w, due to the cross-wind gust, and the irregularity, $\mathbf{w}_d$, due to the guideway. The

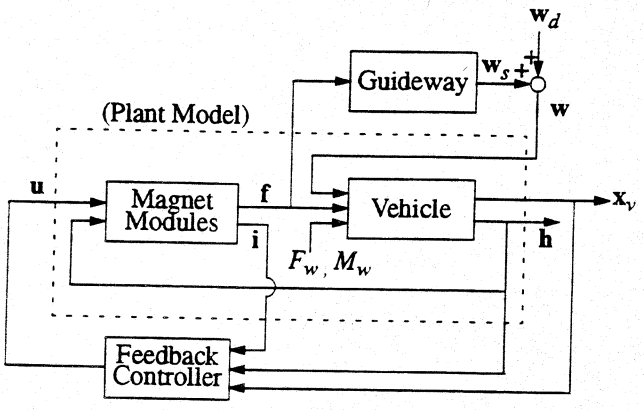

Figure 6. Block Diagram of Complete Maglev System

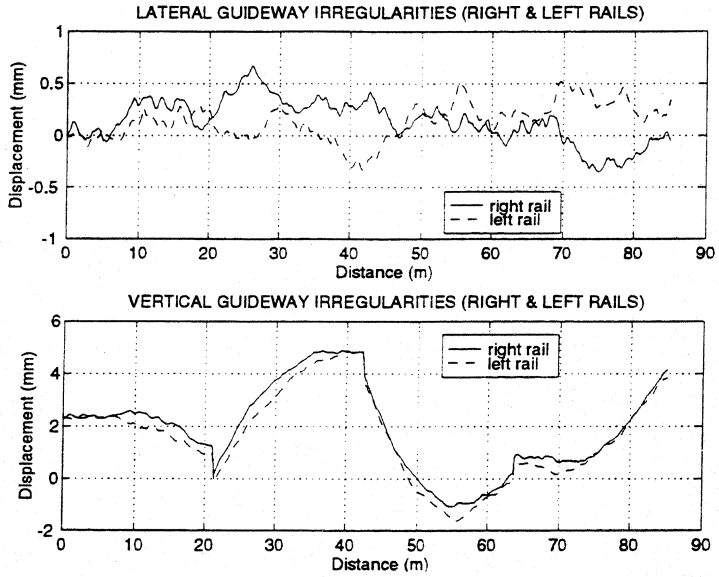

Figure 7. Combined Guideway Irregularities

outputs of the system are the air gap, **h**, and the vehicle state, $\mathbf{x}_v$. In the simulation model, the cross-wind gust is assumed to be a wind profile perpendicular to the guideway with constant velocity. As the vehicle enters the wind zone, the vehicle responds to a sharp discontinuity, such as might occur when the vehicle exits a tunnel. Four types of irregularity characteristics for an elevated guideway have been modeled, including surface roughness, step, ramp, and camber. The simulation model accepts any combination of these guideway irregularities. Since these irregularities result from a wide variety of effects including construction practice and environmental conditions, it is assumed that the amplitudes of each type of irregularity (except for the surface roughness which is described by a power spectral density function) are normally distributed random numbers. With prescribed mean values and standard deviations, the guideway irregularities may represent the tolerance requirements of the guideway structure.

A number of safety- , power- and comfort-related performance measures can be identified for the maglev system developed in this work. The maglev system is required to (*i*) maintain each magnet module/iron rail air gap between 30 mm and 50 mm (*i.e.*, 40 mm nominal gap with ±10 mm maximum gap error), (*ii*) ensure that the control voltages are within a feasible limit of ±300 V, and (*iii*) maximize ride comfort where the ride comfort is measured by comparing carbody accelerations at the car front and rear to the ISO ride quality criteria (ISO, 1978).

In the simulation study, the maglev vehicle was simulated at 500 kph on a 4-span flexible guideway with combined guideway irregularity, consisting of guideway roughness, step, ramp, and camber geometry errors, as shown in Figure 7. The guideway random roughness is described by the power spectral density, $\Phi(\Omega)=A_r/\Omega^2$, with a roughness parameter, $A_r=6.1\times10^{-8}$ m, representing a high quality welded rail. The step deviation, column height, and camber amplitude for each span are generated randomly with a zero mean and a 2 mm standard deviation. We assume no aerodynamic loading in this simulation case. The parameter values for the vehicle model, SC magnet model, and guideway model are summarized in Tables 1, 2, and 3, respectively. The weighting matrices **Q** and **R** used to determine the controller parameters are selected as

$$\mathbf{Q} = \mathrm{diag}\Big(y_{\max}^{-2}, z_{\max}^{-2}, \phi_{\max}^{-2}, \theta_{\max}^{-2}, \psi_{\max}^{-2}, \dot{y}_{\max}^{-2}, \dot{z}_{\max}^{-2}, \omega_{x,\max}^{-2}, \omega_{y,\max}^{-2}, \omega_{z,\max}^{-2}, \dot{i}_{1,\max}^{-2}, \ldots, \dot{i}_{2N_m,\max}^{-2}, y_{I1,\max}^{-2}, \ldots, y_{I(2N_m),\max}^{-2} \Big) \tag{31}$$

$$\mathbf{R} = \mathrm{diag}\Big(u_{1,\max}^{-2}, \ldots, u_{2N_m,\max}^{-2} \Big) \tag{32}$$

where the estimated limits in **Q** and **R** are listed in Table 4.

Table 1. Parameters of Vehicle Model

Parameter	Symbol	Value	Unit
vehicle mass	M_v	30,600	kg
vehicle length	L_v	18	m
vehicle height	h_v	3.9	m
vehicle width	w_v	3.8	m
nominal air gap	h_0	0.04	m
height, magnet centroid to vehicle CG	h_c	1.09	m
width, magnet centroid to vehicle CG	w_c	0.76	m
roll moment of inertia	I_x	7.4×10^4	kg-m^2
pitch moment of inertia	I_y	8.0×10^5	kg-m^2
yaw moment of inertia	I_z	9.6×10^5	kg-m^2
magnet cant angle	β	35	deg
number of modules on each side	N_m	2	None
number of magnets in each module	n_m	12	None

Table 2. Parameters of SC Magnet Model

Parameter	Symbol	Value	Unit
number of turns in SC coil	N_{SC}	1020	None
number of turns in normal coils	N_n	96	None
face area of each magnetic pole	A_m	0.04	m
total resistance of normal coils	R_c	1.0	ohm
permeability of air	μ_0	$4\pi\times10^{-7}$	weber/A-m

Table 3. Parameters of Guideway Model

Parameter	Symbol	Value	Unit
narrow box beam width	w_b	1.2	m
narrow box beam height	h_b	1.8	m
span length	L_s	21.3	m
span mass per unit length	γ	4777	kg-m^2
bending rigidity	EI	1.84×10^{10}	N-m^2
first-mode span damping ratio	ζ	0.03	None

Table 4. Estimated Limits in Weighting Matrices

Parameters	Value	Unit
y_{max}, z_{max}	0.01	m
ϕ_{max}, θ_{max}, ψ_{max}	0.01	rad
$\dot{y}_{max}$, $\dot{z}_{max}$	1.0	m/s
$\omega_{x,\,max}$, $\omega_{y,\,max}$, $\omega_{z,\,max}$	1.0	rad/s
$i_{j,max}$ $(j=1,...,2N_m)$	300	A
$y_{Ij,max}$ $(j=1,...,2N_m)$	0.001	m-s
$u_{j,max}$ $(j=1,...,2N_m)$	300	V

The magnet input voltages at each module are shown in Figure 8. The peak voltage is –49.8 V at module 3 which is substantially less than the limit of –300 V. Figure 9 shows that all the air gap deviations are below the allowable 10 mm safety margin. Figures 10 and 11 depict the vehicle accelerations for the car front and car rear in the lateral and vertical directions, respectively. To evaluate ride comfort, the reduced comfort boundaries of the ISO one hour ride quality criterion are also shown. The results indicate that both the lateral and vertical acceleration levels are below the ISO criterion.

In summary, this simulation study evaluates the maglev system performance under disturbances including guideway flexibility and guideway irregularity. The behavior of the maglev system when exposed to combined disturbances can be determined. For the case studied, the simulation results indicate that the requirements on the air gap safety margin, the control voltage limit, and the ride quality can be satisfied.

5. Conclusions

This paper describes a nonlinear simulation model that was developed to represent the governing behavior of a SC EMS maglev vehicle with a combined lift and guidance system. The simulation model predicts vehicle behaviors under the influence of guideway flexibility, guideway irregularities, and cross-wind gust. An example simulation case of a high-speed vehicle on a guideway with flexibility and a combination of guideway irregularities demonstrates the effectiveness of the LQ optimal controller in satisfying the desired performance specifications.

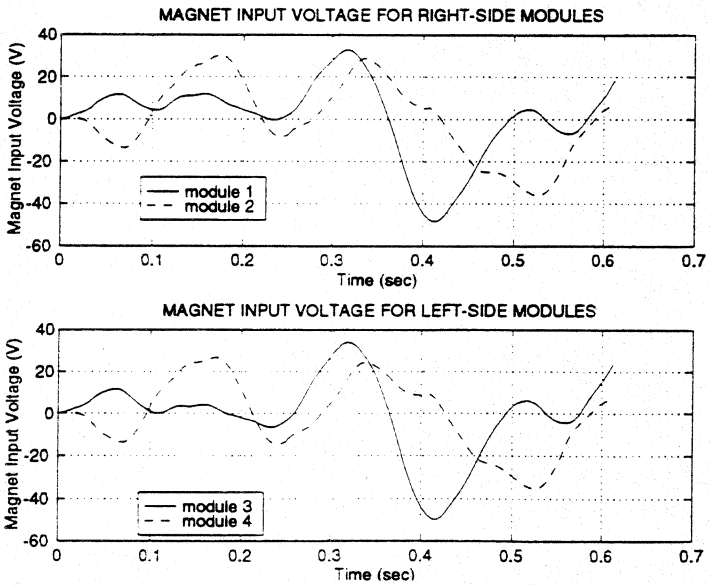

Figure 8. Magnet Input Voltages

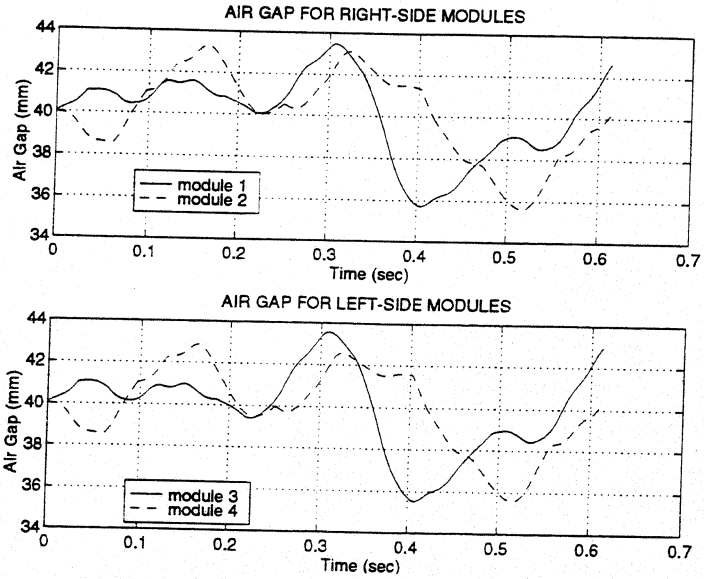

Figure 9. Air Gaps

6. Acknowledgment

The authors are grateful to Mr. D. Tyrell and Dr. H. Weinstock (DOT's Volpe Center, Cambridge, MA), and to engineers at Battelle (Columbus, OH) for their technical contributions. The work described in this paper is based in part on studies performed in support of the Volpe Center activities on the FRA sponsored High Speed Guided Ground Transportation (HSGGT) safety program.

7. References

Cai, Y., Chen, S.S., Rote, D.M., and Coffey, H.T., 1994, "Vehicle/Guideway Interaction for High Speed Vehicles on a Flexible Guideway," *Journal of Sound and Vibration*, Vol. 175, No. 5, pp. 625-646.

Cai, Y., Chen, S.S., Rote, D.M., and Coffey, H.T., 1993, "Vehicle/Guideway Interaction and Ride Comfort in Maglev Systems," *Proceedings of the International Conference on Speedup Technology for Railway and Maglev Vehicles*, Vol. I, Nov. 22-26, Yokohama, Japan, pp. 109-114.

Daniels, L.E., Ahlbeck, D.R., Stekly, Z.J., and Gregorek, G.M., 1992, "Influence of Guideway Flexibility on Maglev Vehicle/Guideway Dynamic Forces," U.S. Department of Transportation Technical Report DOT/FRA/NMI-92/09.

Gran, R. and Proise, M., 1993, "Five Degree of Freedom Analysis of the Grumman Superconducting Electromagnetic Maglev Vehicle Control/Guideway Interaction," *Maglev 93 Conference*, Argonne National Laboratory, May 19-21, Paper No. PS4-6.

ISO, 1978, "Guide for the Evaluation of Human Exposure to Whole-Body Vibration," *ISO Standard 2631*, International Organization for Standardization.

Kortum, W. and Wormley, D.N., 1981, "Dynamic Interactions Between Travelling Vehicles and Guideway Systems," *Vehicle System Dynamics*, Vol. 10, pp. 285-317.

Phelan, R.S., 1993, "High Performance Maglev Guideway Design," *Doctoral Dissertation*, Department of Civil Engineering, Massachusetts Institute of Technology, Cambridge, MA, January.

Proise, M., Deutsch, L., Gran, R., Herbermann, R., Kalsi, S., and Shaw, P., 1993, "System Concept Definition of the Grumman Superconducting Electromagnetic Suspension (EMS) Maglev Design," *Maglev 93 Conference*, Argonne National Laboratory, May 19-21, Paper No. OS4-4.

Smith, C.C. and Wormley, D.N., 1974, "Response of Continuous Periodically Supported Guideway Beams to Traveling Vehicle Loads," ASME Winter Annual Meeting, Paper No. 74-WA/Aut-3, New York, NY, November 17-22.

Wang, S.-K., 1995, "Levitation and Guidance of a Maglev Vehicle Using Optimal Preview Control," *Doctoral Dissertation*, Department of Mechanical Engineering, Carnegie Mellon University, Pittsburgh, PA, May.

Wormley, D.N., Thornton, R.D., Yu, S.-H., and Cheng, S., 1992, "Interactions Between Magnetically Levitated Vehicles and Elevated Guideway Structures," U.S. Department of Transportation Technical Report DOT/FRA/NMI-92/23.

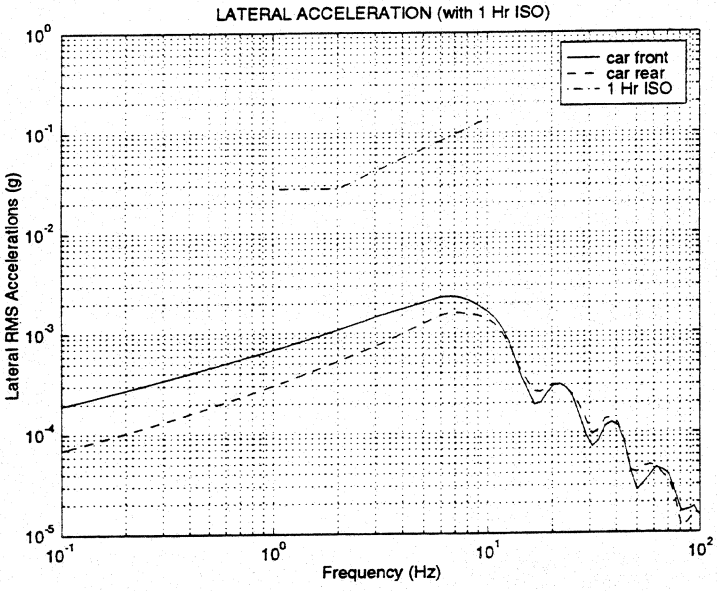

Figure 10. Lateral RMS Accelerations

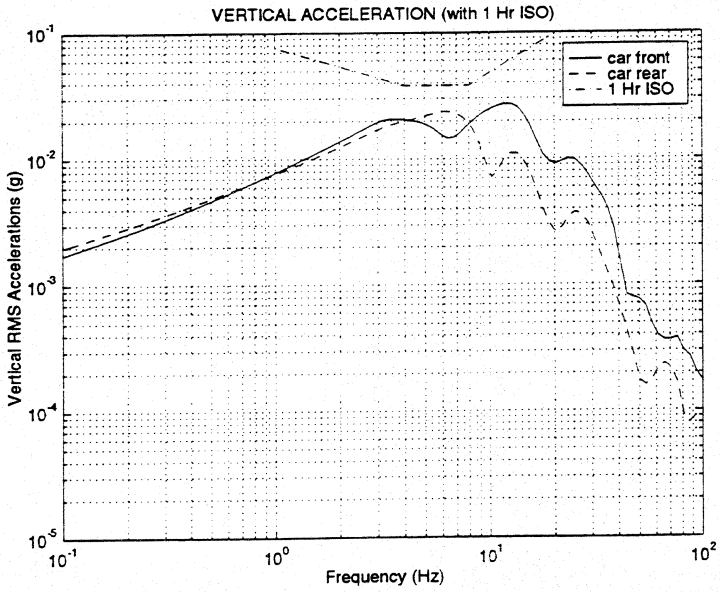

Figure 11. Vertical RMS Accelerations